Biochimica et Biophysica Acta 1828 (2013) 834–844

Contents lists available at SciVerse ScienceDirect

Biochimica et Biophysica Acta

journal homepage: www.elsevier.com/locate/bbamem

Rapid bactericidal action of alpha-mangostin against MRSA as an outcome of membrane targeting

Jun-Jie Koh [a,b,1], Shengxiang Qiu [c,1], Hanxun Zou [a], Rajamani Lakshminarayanan [a], Jianguo Li [a,d], Xiaojun Zhou [c], Charles Tang [e], Padmanabhan Saraswathi [a], Chandra Verma [a,d,f,g], Donald T.H. Tan [a,h], Ai Ling Tan [i], Shouping Liu [a,*], Roger W. Beuerman [a,b,j,**]

[a] Singapore Eye Research Institute, 11 Third Hospital Avenue, 168751, Singapore
[b] Department of Ophthalmology, Yong Loo Lin School of Medicine, National University of Singapore, 119074, Singapore
[c] Program for Natural Products Medicinal Chemistry & Drug Discovery, Key Laboratory of Plant Resources Conservation and Sustainable Utilization, South China Botanical Garden, the Chinese Academy of Sciences, Guangzhou, China
[d] Bioinformatics Institute (A*STAR), 30 Biopolis Street, 07-01 Matrix, 138671, Singapore
[e] Pharmaceutical Microbiology Laboratory, Department of Pathology, Singapore General Hospital, 169608, Singapore
[f] Department of Biological Sciences, National University of Singapore, 14 Science Drive 4, 117543, Singapore
[g] School of Biological Sciences, Nanyang Technological University, 60 Nanyang Drive, 637551, Singapore
[h] Singapore National Eye Center, 168751, Singapore
[i] Department of Pathology, Singapore General Hospital, 169608, Singapore
[j] Duke-NUS Medical School, SRP Neuroscience and Behavioural Division, 169857, Singapore

ARTICLE INFO

Article history:
Received 5 June 2012
Received in revised form 5 September 2012
Accepted 7 September 2012
Available online 13 September 2012

Keywords:
Mangosteen
Garcinia mangostana
α-Mangostin
Antimicrobial
MRSA
Membrane targeting

ABSTRACT

The emergence of methicillin-resistant *Staphylococcus aureus* (MRSA) has created the need for better therapeutic options. In this study, five natural xanthones were extracted and purified from the fruit hull of *Garcinia mangostana* and their antimicrobial properties were investigated. α-Mangostin was identified as the most potent among them against Gram-positive pathogens (MIC = 0.78–1.56 μg/mL) which included two MRSA isolates. α-Mangostin also exhibited rapid *in vitro* bactericidal activity (3-log reduction within 5 min). In a multistep (20 passage) resistance selection study using a MRSA isolated from the eye, no resistance against α-mangostin in the strains tested was observed. Biophysical studies using fluorescence probes for membrane potential and permeability, calcein encapsulated large unilamellar vesicles and scanning electron microscopy showed that α-mangostin rapidly disrupted the integrity of the cytoplasmic membrane leading to loss of intracellular components in a concentration-dependent manner. Molecular dynamic simulations revealed that isoprenyl groups were important to reduce the free energy for the burial of the hydrophobic phenyl ring of α-mangostin into the lipid bilayer of the membrane resulting in membrane breakdown and increased permeability. Thus, we suggest that direct interactions of α-mangostin with the bacterial membrane are responsible for the rapid concentration-dependent membrane disruption and bactericidal action.

Abbreviations: MRSA, methicillin-resistant *Staphylococcus aureus*; EtOAc, ethyl acetate; DOPE, 1,2-di-(9Z-octadecenoyl)-sn-glycero-3-phosphoethanolamine; DOPG, 1,2-dioleoyl-sn-glycero-3-phospho-(1′-rac-glycerol) (sodium salt); CFU, Colony Forming Units; LUV, large unilamellar vesicle; EtBr, ethidium bromide; DiSC3-5, 3,3′-dipropylthiadicarbocyanide iodide; MHB, Mueller Hinton Broth; MIC, minimum inhibitory concentration; DMF, N,N-dimethylformamide; TSA, Tryptic Soy Agar; MD, molecular dynamics; SPC, simple point charge model; HEPES, 4-(2-hydroxyethyl)-1-piperazineethanesulfonic acid; NaCl, sodium chloride; EDTA, ethylenediaminetetraacetic acid; RBC, red blood cell; ATB, Automated force field Topology Builder; SEM, scanning electron microscopy

* Corresponding author. Tel.: +65 6601 2464; fax: +65 6872 3818.
** Correspondence to: R.W. Beuerman, Department of Ophthalmology, Yong Loo Lin School of Medicine, National University of Singapore, 119074, Singapore. Tel.: +65 9821 0846; fax: +65 6322 4599.
E-mail addresses: kohjunjie87@gmail.com (J.-J. Koh), sxqiu@scib.ac.cn (S. Qiu), zouhanxun@gmail.com (H. Zou), lakshminarayanan.rajamani@seri.com.sg (R. Lakshminarayanan), lijg@bii.a-star.edu.sg (J. Li), zxjunxxx@126.com (X. Zhou), tang.chang.chiu@sgh.com.sg (C. Tang), saraswathi.padmanabhan@seri.com.sg (P. Saraswathi), chandra@bii.a-star.edu.sg (C. Verma), snecdt@pacific.net.sg (D.T.H. Tan), tan.ai.ling@sgh.com.sg (A.L. Tan), liushouping@gmail.com (S. Liu), rwbeuerman@gmail.com (R.W. Beuerman).
[1] Equal contribution.

0005-2736/$ – see front matter © 2012 Elsevier B.V. All rights reserved.
http://dx.doi.org/10.1016/j.bbamem.2012.09.004

1. Introduction

Methicillin-resistant *Staphylococcus aureus* (MRSA) is an emergent form of *S. aureus*, which confers resistance to β-lactam antibiotics [1]. MRSA is a predominant source of infections associated with the blood, skin and soft-tissue presenting in US emergency rooms [2,3]. The reduced antibiotic susceptibility of MRSA against the non-β-lactam antimicrobial agents such as mupirocin, clindamycin, vancomycin and daptomycin has also been reported [4–6]. Resistance to antibiotics is widely associated with the failure of treatment, longer hospital stays and greater health care costs [7]. These very current issues have created an urgent need for improved antimicrobial agents against multidrug resistant pathogens such as MRSA [8].

Mangosteen (*Garcinia mangostana*) is a tropical evergreen fruit tree from South East Asia, India and Sri Lanka with a long history of use as a source for traditional medicine for the treatment of chronic diarrhea, infected wounds, skin infections and dysentery [9]. The major bioactive secondary metabolites of mangosteen are xanthone derivatives. These xanthone derivatives have displayed potent pharmacological activities including antibacterial, antifungal, antioxidant, anti-tumoral, anti-inflammatory and anti-allergy properties [9,10]. α-Mangostin, the major extracted derivative has demonstrated active antimicrobial activities against Gram-positive bacteria including *S. aureus* and MRSA [11–16]. In addition, Kaomongkolgit et al. have reported that α-mangostin had no cytotoxic effects on human gingival fibroblasts up to 4000 μg/mL [17].

Antibacterial action of α-mangostin was first studied by Nguyen and Marquis. They reported that the antimicrobial action of α-mangostin was from targeting cytoplasmic enzymes [18]. However, the action of enzyme targeted antimicrobials would be expected to require considerable time [19], which seems in contrast to the reported rapid bactericidal action of α-mangostin [18]. The rapid antimicrobial action is suggestive of the antimicrobial action of the natural antimicrobial peptides or peptidomimetics which act on bacterial membrane [20–22]. Therefore, we hypothesized that the bacterial membrane is the primary target of α-mangostin and the results of our studies provide support for this suggestion. The aim of this study was to provide a detailed analysis of the antibacterial action of α-mangostin against Gram-positive bacteria using a combination of biophysical, biochemical and computational studies. Understanding the antibacterial action of α-mangostin could provide critical information for rational design of more potent xanthone based antimicrobials.

2. Materials and methods

2.1. Extraction, isolation and characterization

The five xanthones (Fig. 1), 1,5,8-trihydroxy-3-methoxy-2-(3-methyl-2-butenyl)xanthone (SZ-1), γ-mangostin (SZ-2), garcinone E (SZ-3), α-mangostin (SZ-4) and mangostenone D (SZ-5), were isolated and the details of the isolation and the structure of these compounds have been reported previously [23,24]. Briefly, the oven-dried and milled fruit hull (5 kg) of *G. mangostana* (imported from Thailand) was extracted with 95% ethanol (3 × 8 L) at room temperature, for 3 days each. After evaporation of the solvent in vacuum, the pooled crude ethanolic extract was suspended in H_2O (2 L) which appeared as brown syrup, which was then partitioned with EtOAc (3 × 2 L) to obtain an EtOAc-soluble fraction. The EtOAc-soluble extract was subjected to chromatography over a silica gel column eluted with a mixture of petroleum ether (PE) and acetone with increasing polarity (ratio of PE/acetone from 10:1 to 1:1). SZ-4 was obtained as a yellow solid from the solution (ratio of petroleum ether/acetone 8:1) and recrystallized with PE–acetone. SZ-2 was obtained as a yellow powder from the solution (petroleum ether (PE)–acetone 5:1) followed by further purification over a Sephadex LH-20 column using methanol as solvent. SZ-1, SZ-3 and SZ-5 were obtained from the PE/acetone (6:1), PE/acetone (7:1) and PE/acetone (7:2) eluting fractions, respectively, by repeated column chromatography over silica gel eluted with gradient solvent mixture (PE–acetone) with increasing polarity (%Acetone from 0 to 100%), followed by further purification using Sephadex LH-20 eluted with methanol. The structures of SZ-1, 2, 3, 4 and 5 were readily assigned to 1,5,8-trihydroxy-3-methoxy-2-(3-methyl-2-butenyl)xanthone [25], γ-mangostin [26], garcinone E [27], α-mangostin [28] and mangostenone D [29], respectively by comparison of their NMR spectral data with those reported in the literature. Purities of SZ-1 to SZ-5 were 98.7%, 99.2%, 98.8% and 99.8% and 99.0% respectively, determined by HPLC.

2.2. Antimicrobials and chemicals

α-Mangostin was extracted and purified as described above. Daptomycin was purchased from Tocris Bioscience, United Kingdom. Vancomycin hydrochloride was the 2nd ASEAN Reference Standard (ARS) and obtained from the ARS Singapore representative. All phospholipids were purchased from Avanti Polar Lipids, Inc. (Alabaster, AL). Phospholipids used in this study were 1,2-di-(9Z-octadecenoyl)-sn-glycero-3-phosphoethanolamine (DOPE) and 1,2-dioleoyl-sn-glycero-3-phospho-(1′-*rac*-glycerol) (sodium salt) (DOPG). The stock solution of vancomycin was prepared by dissolving and diluting in purified water to make up to 1000 μg/ml and stored frozen at −24 °C. All chemicals used were purchased from Sigma Aldrich unless otherwise stated.

2.3. Bacterial strains and growth condition

The bacterial strains used in these studies were *S. aureus* ATCC29213, *Bacillus cereus* ATCC11778, *Enterococcus faecalis* ATCC29212, and three MRSA clinical isolates: DM21455 (from eye), DM09808R (from eye), and DB57964/04 (from blood). All strains used were not more than four passages removed from the original master stock obtained from the American Type Culture Collection or from our clinical isolate collection. The direct colony suspension method described by the Clinical and Laboratory Standards Institute (CLSI) was used for inoculum preparation. Inoculum suspensions were made from isolated colonies selected from an 18- to 20-h/35 °C Tryptic Soy Agar (TSA) plates. Bacterial strains used in antibacterial action studies were suspended in HEPES buffer (5 mM HEPES, pH 7).

2.4. Susceptibility testing

The stock solution of α-mangostin used in the studies was first dissolved in N,N-dimethylformamide (DMF) and then diluted in purified water to make up to 1000 μg/ml and stored frozen at −20 °C. MIC determinations were performed using the broth macro-dilution method as described by the CLSI. Serial twofold dilutions of

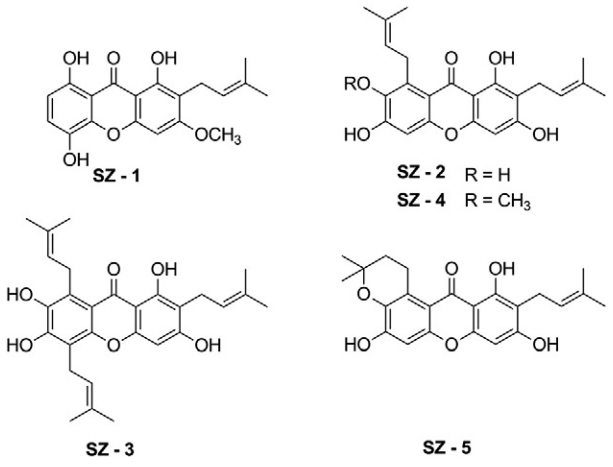

Fig. 1. Five natural xanthones extracted from hull of *G. mangostana*. Chemical structure of five natural xanthones extracted from hull of *G. mangostana*.

α-mangostin, daptomycin or vancomycin solutions were prepared in Mueller Hinton Broth (MHB), cation adjusted (MHB) in test tubes. The inoculum was prepared by making a direct MHB suspension of isolated colonies selected from the 18–20 h Tryptic Soy Agar (TSA) plate. The concentration of the inoculum suspension was adjusted with MHB. After inoculation, each tube contained approximately 5×10^5 Colony Forming Units (CFU)/mL. The tubes were then incubated at 35 °C for 22 h. The organisms used in the MIC studies are listed in Table 1.

2.5. Time-kill kinetics

The inoculum was prepared by making a direct suspension of isolated colonies selected from the 18–20 h Tryptic Soy Agar (TSA) plate in 0.31 mM phosphate buffer (0.31 mM monobasic potassium; pH 7.2). The concentration of the inoculum suspension was adjusted with the buffer. After inoculation, each tube with the desired concentration of α-mangostin or vancomycin solution also contained bacteria at 10^5 to 10^6 CFU/mL. The tubes were then incubated at 35 °C and samples were withdrawn at the specified time intervals for viable plate counts. Serial 10-fold dilutions of the sample were made in the diluent, D/E Neutralisation Broth. A 20 μL aliquot of each dilution was plated out on TSA plates using the surface-spread plate method. The plates were incubated at 35 °C for 48 to 72 h. The possibility of carry-over of the antimicrobial agents onto the plates was examined using the test organism as control in the serial dilutions in the presence and absence of the antimicrobial agents. The detection limit of reliable viable plate count was found to be 10 CFU/ml for α-mangostin and 100 CFU/ml for vancomycin.

2.6. Multipassage resistance selection studies

Membrane targeted activity of α-mangostin may be expected to avoid the development of resistance. Multipassage resistance selection studies were carried out to test this idea using α-mangostin with *E. faecalis* (ATCC29212) and MRSA (DM21455). The development of resistance of these organisms against α-mangostin was measured based on the progressive increase in the MIC of the bacteria over time (passages). After 20 to 22 h of incubation, bacterial growth was checked and bacteria that grew in the highest concentration were re-passaged in a fresh dilution series of the antimicrobial agents. The process was repeated every 20 to 22 h for up to 20 passages and the MICs were determined at every passage as specified earlier. Resistance was defined as an increase in original MIC of more than 4 fold [30].

2.7. Cytoplasmic membrane depolarization assay

The effect of α-mangostin on the membrane potential of clinical isolate *S. aureus* (DM4001) was probed by membrane sensitive $DiSC_3$-5 fluorescent assay based on the modified method of Wu and Hancock [31]. Briefly, *S. aureus* was harvested at an early exponential growth phase and washed with buffer solution (5 mM HEPES at pH 7) and resuspended in the same buffer until an optical density of 0.09 at 620 nm [OD620] was obtained. The cell suspension was incubated with 0.4 μM $DiSC_3$-5 (Invitrogen) and 0.1 M potassium chloride (KCl) solution at 37 °C until $DiSC_3$-5 uptake was maximal (when the reduction of fluorescence intensity was stable due to self-quenching of $DiSC_3$-5 in the untreated bacteria). The desired concentration of α-mangostin was added into a stirred cuvette. The fluorescence reading was monitored for 500 s with a Photon Technology International Model 814 fluorescence spectrophotometer, at an excitation wavelength of 660 nm and an emission wavelength of 675 nm. DMF alone had no effect on depolarization. Experiments were repeated at least three times and were reproducible. Data from one experiment is presented.

2.8. EtBr uptake assay

Cytoplasmic membrane disruption was determined by using ethidium bromide (EtBr). EtBr is a membrane impermeable dye and is a DNA intercalating agent. When the integrity of inner membrane was disrupted, EtBr may bind to DNA in the cell and fluoresces more strongly when exposed to UV light. *S. aureus* with $OD_{620} = 0.09$ was prepared as for the cytoplasmic membrane depolarization assay as described above. The cell suspension was incubated with 17 nM EtBr at 37 °C until the fluorescence reading was stable. Then, the desired concentration of an antimicrobial was added and the fluorescence reading was monitored for 500 s at an excitation wavelength of 360 nm and an emission wavelength of 616 nm using Photon Technology International Model 814 fluorescence spectrophotometer. DMF alone had no effect on EtBr fluorescence and membrane permeability. Triton X-100 (40%) was used to maximize the permeabilization effect. Experiments were repeated at least three times and yielded reproducible results. Results from one experiment are presented.

2.9. SYTOX green assay

To further investigate the effect of α-mangostin on the bacterial membrane, another membrane impermeable dye, SYTOX green (Invitrogen) was used. Similar to the EtBr, SYTOX green fluoresces strongly when it interacts with nucleic acids. *S. aureus* with $OD_{620} = 0.2$ was prepared and suspended in 40 mM PBS (100 mM NaCl, pH 7) as for the EtBr uptake assay described above. The cell suspension was incubated with 3 μM of SYTOX green for 5 min. Then, the desired concentration of α-mangostin was added and the fluorescence was monitored for 800 s with at an excitation wavelength of 504 nm and an emission wavelength of 523 nm. DMF alone had no effect on SYTOX Green fluorescence. Melittin (10 μg/mL; cell lytic factor; EZBiolab, USA) was used as a positive control. Experiments were repeated at least three times and were reproducible. Data from one experiment is presented.

2.10. Calcein leakage experiment

Leakage from large unilamellar vesicles (LUV) was monitored by the release of calcein encapsulated in the LUVs as described [32,33]. In brief, the lipids (DOPE/DOPG = 75/25) were dissolved in methanol/chloroform (1:2, by volume). The solvent was dried gently using a constant stream of nitrogen gas. Then, the lipid film was placed under vacuum for at least 2 h. The dried lipid film was hydrated with calcein solution (80 mM calcein, 50 mM HEPES, 100 mM NaCl, 0.3 mM EDTA, pH 7.4) to a final lipid concentration of 30 mM. The hydrated vesicles were frozen in liquid nitrogen and warmed in water bath for 7 cycles. Homogeneous LUVs with 100 nm were then prepared by the extrusion method using a mini-extruder (Avanti Polar

Table 1
In vitro antimicrobial activities of mangosteen extracts (SZ-1–SZ-5) against Gram-positive bacteria.

Bacteria	MIC (μg/mL)					
	SZ-1	SZ-2	SZ-3	SZ-4	SZ-5	Van[a]
S. aureus DM21455[b]	>12.5	3.125	3.125	1.56	>12.5	0.78
S. aureus DM09808R[b]	>12.5	12.5	3.125	1.56	>12.5	1.56
B. cereus ATCC11778	>12.5	1.56	3.125	1.56	>12.5	1.56
MRSA DB57964/04	ND[c]	1.56	ND	1.56	ND	ND
S. aureus ATCC29213	ND	1.56	ND	0.78	ND	1.56

[a] Vancomycin.
[b] Clinical isolate strains.
[c] Not determine.

Lipid Inc.), as described in the Avanti Polar Lipid Inc. website [34]. The extrusion was done for 10 cycles using a polycarbonate membrane (Whatman, pore size 100 nm). Calcein encapsulated vesicles were separated from free calcein with gel filtration column using Sephadex G-50. The concentration of eluted liposomes was determined using a total phosphorus determination assay as described by Avanti Polar Lipids, Inc. website [35]. Calcein leakage was monitored using a Photon Technology International Model 814 fluorescence spectrophotometer, at an excitation wavelength of 490 nm and an emission wavelength of 520 nm. An aliquot of the LUV suspension was added into a stirred cuvette at various concentrations of an α-mangostin solution in DMF to obtain the desired lipid to α-mangostin ratios of 2, 4 and 8. The final concentration of lipid was 50 μM and the final percentage of DMF is <0.2%. 0.1% Triton X-100 was added to determine the intensity at complete leakage. Control experiment using 0.2% of DMF demonstrated that leakage of calcein from the LUVs was not observed. Percentage of leakage (%L) was calculated with $\%L = [(I_t - I_0)/(I_\infty - I_0)] * 100]$, where I_0 and I_t are intensities before and after addition of α-mangostin respectively and I_∞ is intensity after addition of 0.1% triton X-100.

2.11. Visualization of bacterial membrane permeation

Clinical isolate *S. aureus* DM4001 was suspended in HEPES buffer (5 mM) until the OD_{620} of 0.4 was obtained. The suspension was incubated with 1.56 μg/mL (1× MIC) and 6.25 μg/mL (4× MIC) respectively for 20 min with 3 μM of SYTOX green. Then, the *S. aureus* were immobilized on poly(L-lysine)-coated glass slides. The slides were examined by fluorescence microscope (ZEISS Model Axioplan 2IE) with an excitation wavelength of 485 nm. Bacterial treatment with vancomycin (6.25 μg/mL) was used as control.

2.12. Scanning electron microscopy (SEM)

For the electron microscopy analysis, *S. aureus* DM 4001 was grown on TSA Plates overnight and a suspension of 10^8 CFU/ml was prepared in United States Pharmacopeia Buffer (USP Phosphate buffer). The suspension was centrifuged at 3000 rpm for 20 min and the pellet was washed with the same buffer. An aliquot of the bacterial suspension was incubated with 10 μg/ml of α-mangostin at 35 °C for 30 min. After incubation, the bacterial suspension was again centrifuged, washed and prefixed in 0.5 ml of a mixed aldehyde fixative (2% glutaraldehyde and 2% paraformaldehyde in 0.1 M sodium cacodylate buffer, pH 7.2) for 24 h. Then the suspension was washed once again in sodium cacodylate buffer (Electron Microscopy Sciences, Washington, USA) and subsequently mounted on poly-L-Lysine coated cover-slips and post-fixed in 1% osmium tetroxide (Electron Microscopy Sciences). Following dehydration in a graded series of ethanol, the samples were critical-point-dried and sputter coated with 10 nm of gold. All samples were viewed and photographed on a Philips XL30-FEG-SEM (FEI Electron Optics BV, Eindoven, The Netherlands) at an accelerating voltage of 10 kV at the Electron Microscopy Unit, National University of Singapore. Bacteria incubated in USP phosphate buffer without the addition of α-mangostin was used as a control and processed in the same manner and photographed.

2.13. Hemolysis

The hemolytic activity of α-mangostin was determined by the amount of hemoglobin that was released from rabbit erythrocytes. Fresh rabbit red blood cells (RBCs) were isolated from the whole blood of New Zealand white rabbits, which was approved by the IACUC of SingHealth and were according to the standards of the Association for Research in Vision and Ophthalmology. The blood was centrifuged at 3000 rpm for 10 min. Then, RBCs were further washed with sterile PBS for 2 times and diluted to 8% (v/v) stock solution in sterile PBS. α-Mangostin was dissolved in DMSO and mixed with RBCs to prepare the desired concentration of α-mangostin in RBCs (final v/v of RBCs = 4%). Final v/v of DMSO in the RBC suspension was at 0.5%, which had negligible effect on RBCs. The RBC suspensions were then added to 96-well plates and incubated at 37 °C for 60 min. After incubation, the RBC suspensions were centrifuged at 3000 rpm for 3 min. The supernatant (100 μL) was transferred into a clean 96-well plate and the amount of hemoglobin liberated was determined by measuring the absorbance (abs) at 576 nm with TECAN infinite 200 microplate reader. 2% Triton X-100 and PBS were used as positive and negative control, respectively. Percent of hemolysis was calculated using equation as below:

$$\%\ \text{Hemolysis} = \frac{\text{Mixtureabs}_{576\ \text{nm}} - \text{Negativecontrolabs}_{576\ \text{nm}}}{\text{Positivecontrolabs}_{576\ \text{nm}} - \text{Negativecontrolabs}_{576\ \text{nm}}} \times 100.$$

2.14. Molecular dynamic (MD) simulations

Molecular models of the interactions of α-mangostin with model bacterial membranes in the presence of solvent water were constructed *in silico* and studied using molecular dynamics (MD) simulations. Although the lipid composition of the inner membrane of different bacteria varies, the major components in the bacterial inner membrane are POPE (1-Palmitoyl-2-oleoyl-sn-glycero-3-phosphoethanolamine) and POPG (1-palmitoyl-2-oleoyl-sn-glycero-3-phosphoglycerol) [36]. Thus we used 128 mixed lipid molecules with a ratio of POPG/POPE = 3/1 to represent and capture the general model of bacterial membrane [37]. Both α-mangostin and lipid molecules were modeled using the Gromos53a6 force field [38] and solvent water molecules were modeled using the simple point charge model (SPC) [39]. The parameters of α-mangostin were generated using the Automated force field Topology Builder (ATB) [40]. Two simulations were carried out, using 1 and 9 α-mangostin molecules, corresponding to low and high concentrations of α-mangostin. In both simulations, α-mangostin molecules with random orientations were put close to the model bacterial membrane. Then the system was solvated with about 7200 water molecules and neutralized with sodium ions. Before the production stage of the MD simulation, the system was subjected to 500 steps of energy minimization using the steep descent algorithm, followed by 10 ps NVT simulation. Then a 250 ns MD simulation was performed for both cases, corresponding to different concentrations of α-mangostin. To enhance sampling of the conformations of α-mongostin at a certain distance from the bilayer center, a series of distance-restrained simulations was carried out by fixing the distance between one α-mangostin and the bilayer center, using the pull module of gromacs [41]. During all MD simulations, a cut-off distance of 1.2 nm was used for both the LJ and real-space electrostatic interactions, and the particle-mesh Ewald algorithm was employed to calculate the long-range electrostatic interactions in reciprocal space. The Nose–Hoover method was used to maintain the target temperature at 310 K and Parrinello–Rahman method with semi-isotropic coupling was used for maintaining the pressure at 1 atm in the NPT ensemble.

3. Results

3.1. Antimicrobial activity of xanthones extracted from mangosteen

In vitro antimicrobial activities of the five natural xanthones isolated from the hull of mangosteen fruit (Table 1) demonstrated that α-mangostin was the most potent of the plant extracts after screening against Gram-positive bacteria, as MIC values were 0.78–1.56 μg/mL. In contrast, gamma-mangostin (SZ-2) and garcinone E (SZ-3) had higher MIC values (MICs 3.125–12.5 μg/mL), while mangostenone D (SZ-5) and 1,5,8-trihydroxy-3-methoxy-2-(3-methyl-2-

butenyl)xanthone (SZ-1) were not active even at 12.5 μg/mL. MIC levels for α-mangostin (SZ-4) were comparable to vancomycin for *B. cereus*, *S. aureus* as well as several isolates of MRSA (MIC = 1.56 μg/mL for all the strains tested). MIC values for vancomycin were within CLSI published ranges [42]. Comparing the structures of SZ-1 to SZ-5, the presence of an isoprenyl group at the carbon-8 position may play an important role in conferring antimicrobial activity since molecules that lack this moiety (SZ-1) or cyclized to the adjacent carbon (SZ-5) displayed poor antimicrobial properties.

3.2. Time killing assay

To understand the nature of the action against Gram-positive bacteria, time killing analyses were carried out using ATCC strains and clinical isolates of *S. aureus*. α-Mangostin displayed rapid, concentration-dependent killing of MRSA (09808R), at concentrations of 2× MIC or 4× MIC levels achieving 3-log and 5-log reductions respectively in viable counts within 5 min (Fig. 2A). At concentrations below 1× MIC, less than a 3-log reduction of viable counts was attained. Similar findings were observed when another MRSA (DM21455) and *B. cereus* (ATCC11778) were tested and rapid killing of over >3 log CFU/mL was found at the concentration of 3 μg/mL in 5 min (Fig. 2B). Vancomycin had notably poorer bactericidal activity against MRSA (DM21455) and *B. cereus* (ATCC11778) at 2× MIC or 8× MIC. There was no significant (≥3-log) reduction in viable cells even after 300 min of incubation with vancomycin at 8× MIC (Fig. 2C). Vancomycin is bactericidal against *S. aureus* and kills in a time-dependent manner [43]. A previous report has shown that 16–20 h is needed to achieve a 3-log reduction of the bacterial inoculum [44]. By comparison α-mangostin has rapid bactericidal action.

3.3. Multistep resistance selection

Antibiotic resistance is defined as more than a 4-fold increase in original MIC [30]. To examine this issue, a laboratory simulation of resistance using *E. faecalis* ATCC29212 and MRSA DM21455 was carried out and these organisms were individually incubated with α-mangostin. Resistance was not seen to develop for *E. faecalis* which had less than a >4-fold MIC increase for α-mangostin (MIC at passage 0, 0.78 μg/mL; MIC at passage 20, 1.56 μg/mL). 2-fold increase in MIC was observed for MRSA DM21455 from passage 10–19 (Fig. 3). However, the 2-fold increase was not stable throughout the experiment and was within the error margin for MIC testing. Overall, there was no evidence for the emergence of mutational resistance of the two tested strains of *E. faecalis* and MRSA against α-mangostin.

3.4. α-Mangostin depolarizes the bacterial membrane

α-Mangostin showed rapid killing action, which is similar to the natural antimicrobial peptides [45]. From this observation, a membrane targeted antibacterial action is expected. $DiSC_3$-5 is a cytoplasmic membrane potential sensitive dye. Partitioning of $DiSC_3$-5 onto the surface of a polarized cell self quenches its fluorescence. Depolarization prevents dye partitioning on the cell surface and releases the dye into the media with a concomitant increase in fluorescence intensity. Thus, the increase in fluorescence intensity of $DiSC_3$-5 would be proportional to the degree of membrane potential reduction [31]. Addition of α-mangostin to the clinical isolate *S. aureus* DM4001 caused a rapid, concentration-dependent increase in fluorescence intensity of $DiSC_3$-5, indicating loss of membrane potential (Fig. 4). Fluorescence signals from bacteria exposed to higher concentrations of α-mangostin at 2×, 4× and 8× MIC concentrations showed a sharper, immediate increase. The extent of depolarization at 8× MIC was very similar to 4× MIC as α-mangostin at 4× MIC was able to completely dissipate the membrane potential. Cells exposed to 1× MIC lost membrane potential gradually. In contrast, no depolarization was observed at α-mangostin concentrations lower than the MIC.

3.5. Ethidium bromide (EtBr) uptake assay

The membrane interaction study was continued using EtBr, a membrane impermeable dye which is generally excluded from bacteria with intact membranes. The dye intercalates into double-stranded nucleic acids with enhanced fluorescence in the visible region. Membrane disruption by α-mangostin allowed the influx of the dye to complex with intracellular nucleic acids with increased fluorescence intensity. Addition of α-mangostin at concentrations of 2× MIC, 4× MIC and 8× MIC to the clinical strain of *S. aureus* resulted in a strong increase in the emission intensity of EtBr at 616 nm (Fig. 5A). Addition of α-mangostin at concentrations lower than MIC did not display significant enhancement of EtBr fluorescence. Controls without antimicrobial treatment, membrane-targeting antibiotics such as daptomycin and

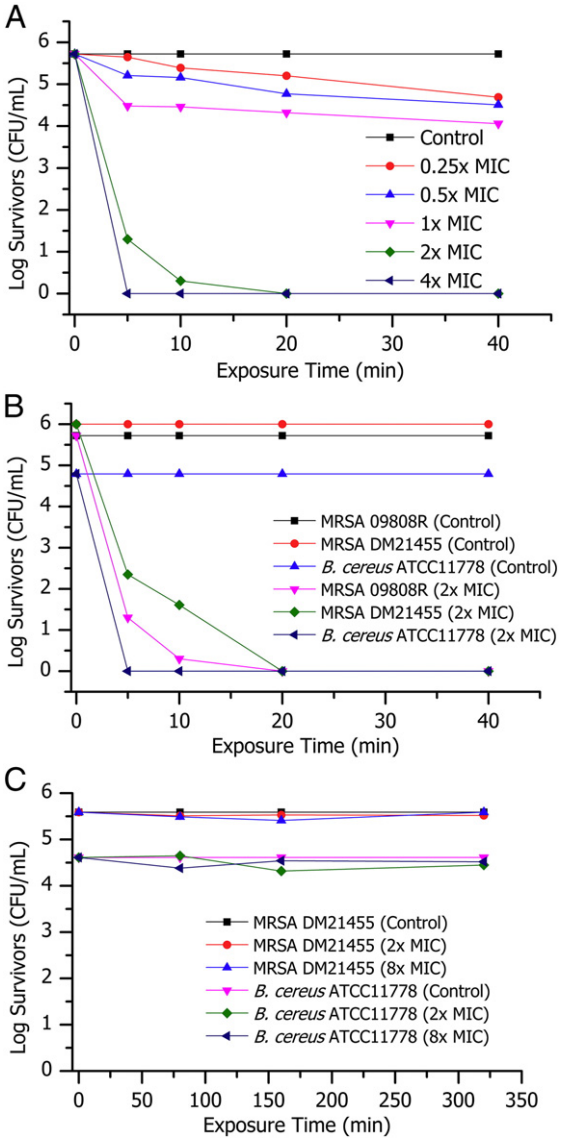

Fig. 2. Time-kill kinetics of MRSA and *B. cereus* using α-mangostin and vancomycin as comparator. (2A) Concentration-dependent bactericidal killing curve of MRSA (09808R) using α-mangostin. Effect of (2B) α-mangostin and (2C) vancomycin on the survival of MRSA and *B. cereus*. MIC values (μg/mL): α-mangostin = 1.56; vancomycin = 1.56. Limit of detection: $\log_{10}$ CFU/mL = 1 for α-mangostin and $\log_{10}$ CFU/mL = 2 for vancomycin.

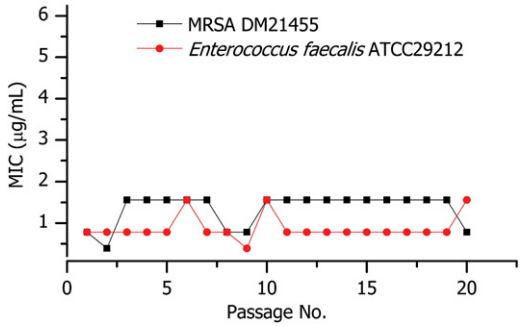

Fig. 3. Multipassage resistance selection studies of α-mangostin. Plot of MIC (μg/mL) of α-mangostin against *E. faecalis* ATCC29212 and MRSA DM21455 during 20 serial passages. No 4-fold increase of MIC was observed. However, a 2-fold increase of MIC value for MRSA was observed from passage 10–19.

vancomycin did not result in an increased intensity of EtBr fluorescence (Fig. 5B). As expected, addition of Triton X-100 (40%) as a positive control (Bio-Rad laboratories) rapidly permeabilized the bacterial membrane allowing entrance of EtBr, which complexed with nucleic acids and fluoresced.

3.6. SYTOX green assay

We further investigated the membrane disruption action of α-mangostin using SYTOX green dye. Addition of α-mangostin to the clinical isolate *S. aureus* DM4001 caused concentration-dependent increase in fluorescence intensity of SYTOX green indicating that the membrane was permeabilized (Fig. 6). Addition of α-mangostin at concentrations of 2× MIC and 4× MIC resulted in a strong increase in the emission intensity of SYTOX green fluorescence emission. Cells exposed to 0.5× and 1× MIC increased the SYTOX green fluorescence emission gradually. In contrast, no increase of fluorescence emission was observed at α-mangostin concentrations at 0.25× MIC (Fig. 6). Melittin is a principal peptide of bee venom with strong membrane lytic property [46]. Addition of 10 μg/mL of melittin caused a rapid increase in fluorescence intensity of SYTOX green, indicating that the cells were permeabilized rapidly. The result demonstrated that α-mangostin has similar membrane permeabilization effect to melittin. Therefore, the SYTOX green assay further shows that α-mangostin is membrane targeting.

3.7. α-Mangostin induced leakage from calcein-loaded LUVs

We constructed artificial bacterial membrane containing 75/25 DOPE/DOPG lipids to further investigate the membrane targeting properties of α-mangostin. Dye leakage from the LUVs showed that α-mangostin could induce ~37% leakage at a lipid-to-α-mangostin ratio of 2. The lytic activity at lipid-to-α-mangostin ratio of 4 was ~28% and ~16% at the ratio of 8 (Fig. 7). The results showed that α-mangostin could interact with artificial bacterial membranes and induced vesicle lysis.

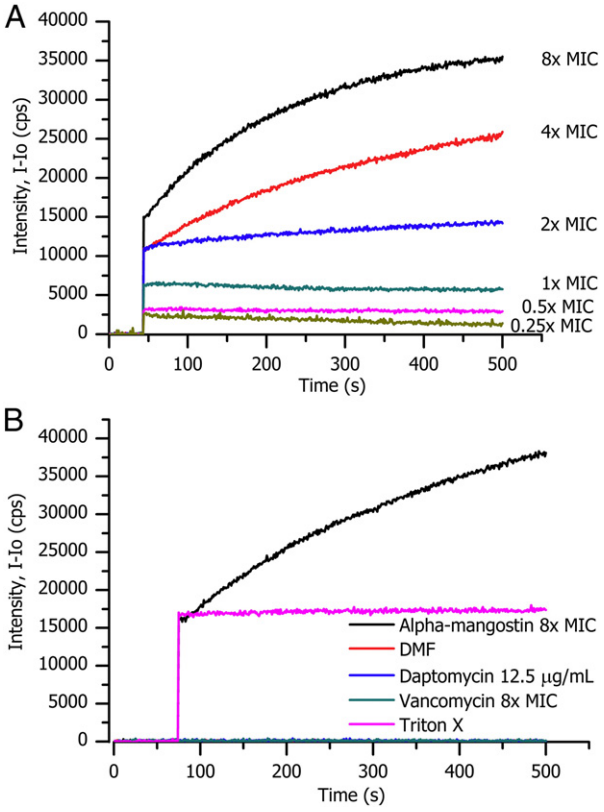

Fig. 5. α-Mangostin as a cytoplasmic membrane disruption agent. (A) Effects of α-mangostin with different concentrations on the fluorescence intensity of EtBr incubated with clinical isolate *S. aureus* DM4001 at 0.25×, 0.5×, 1×, 2×, 4× and 8× MICs. (B) Effects of different antibiotics on the EtBr fluorescence intensity: red line, 1 μL DMF; black line, α-mangostin, 8× MIC; blue line, daptomycin, 12.5 μg/mL; light blue line, vancomycin, 8× MIC; and purple line, 15 μL triton X-100. MIC values (μg/mL): α-mangostin = 1.56; vancomycin = 1.56. cps: count per second.

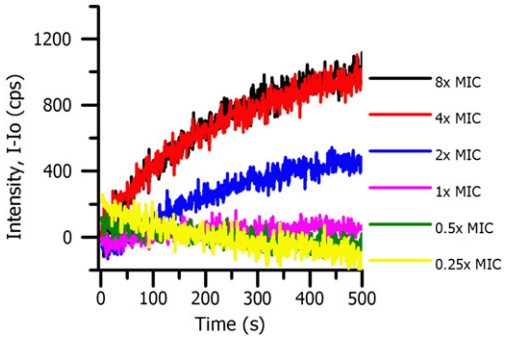

Fig. 4. α-Mangostin induced membrane depolarization of Gram-positive bacteria. (3A) Effects of α-mangostin on the fluorescence intensity of $DiSC_3$-5 in the presence of clinical isolate *S. aureus* DM4001. α-Mangostin was added when the intensity of $DiSC_3$-5 is stable at 0.25× MIC–8× MIC. MIC values (μg/mL): α-mangostin = 1.56. cps. count per second.

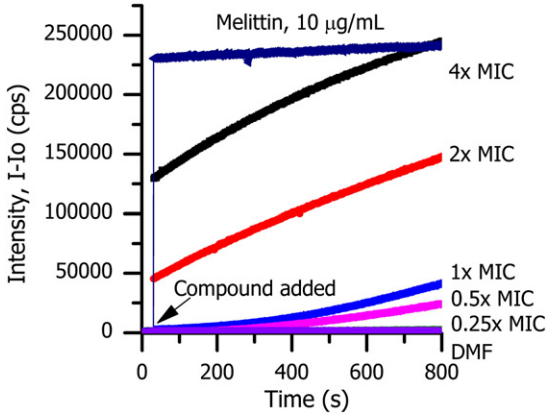

Fig. 6. SYTOX green assay further shows that α-mangostin is membrane active agent. Effects of α-mangostin at 0.25×, 0.5×, 1×, 2× and 4× MICs to the clinical isolate *S. aureus* DM4001 incubated with SYTOX green. Dark blue line: Melittin (10 μg/mL). Addition of DMF (green line) and 0.25× MIC (purple line) had no effect on the SYTOX green fluorescence emission.

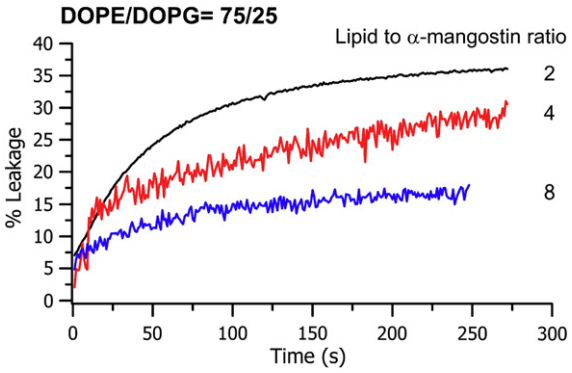

Fig. 7. α-Mangostin induced leakage of artificial bacterial membrane. Percent released of calcein from 75/25 DOPE/DOPG LUVs upon addition of lipid to α-mangostin ratios of 4 and 8.

3.8. Visualization of permeation of bacterial membranes

The cationic dye SYTOX green (Invitrogen) is a membrane impermeable dye. When the bacterial membrane is disrupted, SYTOX green levels will increase in the cytoplasm, resulting in bound fluorophore to intracellular nucleic acids, which can be visualized using fluorescence microscopy. Fig. 8 shows that when the clinical isolate, DM4001 of *S. aureus* was exposed to 3.125 μg/mL (2× MIC) and 6.25 μg/mL (4× MIC) of α-mangostin, in the presence of SYTOX green, a marked fluorescence signal within the bacteria could be observed. The results suggested that α-mangostin disrupted the bacterial membrane rapidly. Untreated controls or bacteria treated with vancomycin at 6.25 μg/mL did not show similar levels of fluorescence.

3.9. Visualization of cell damage by using scanning electron microscopy

Morphological changes were visualized with scanning electron microscope. *S. aureus* (DM4001) treated with α-mangostin were compared with untreated controls. Untreated cells had intact, smooth and spherical morphology (Fig. 9A and C). In contrast, bacteria exposed to 10 μg/mL of α-mangostin showed significant changes. Numerous lysed cells accompanied by cellular debris and release of intracellular components were observed. In addition, some cells had burst with deep craters on the cell walls compatible with the idea of a membrane targeted action mechanism (Fig. 9B and D).

3.10. Selectivity study using rabbit red blood cells

To investigate the effect of α-mangostin on the mammalian membrane, we determined the lytic effect of α-mangostin using rabbit RBCs. Fig. 10 shows that at MIC and bactericidal concentrations (2× and 4× MIC), the % hemolyses were 7.7 +/− 2.4%, 8.1 +/− 1.9% and 10.5 +/− 4.8% respectively (Fig. 10). The result demonstrates that α-mangostin has good selectivity against bacterial membrane at MIC and bactericidal concentrations.

3.11. Molecular dynamic (MD) simulations

To understand membrane disruption on an atomic level, we used MD simulations to provide information on membrane penetration pathways of α-mangostin using a model bacterial membrane. We determined the penetration properties of α-mangostin into POPE/POPG (75/25) bilayers using all-atom MD simulations. When α-mangostin was placed close to the bacterial membrane, a rapid absorption of the molecule into the membrane was observed. At a low drug/lipid ratio (1/128), the distance between α-mangostin and the

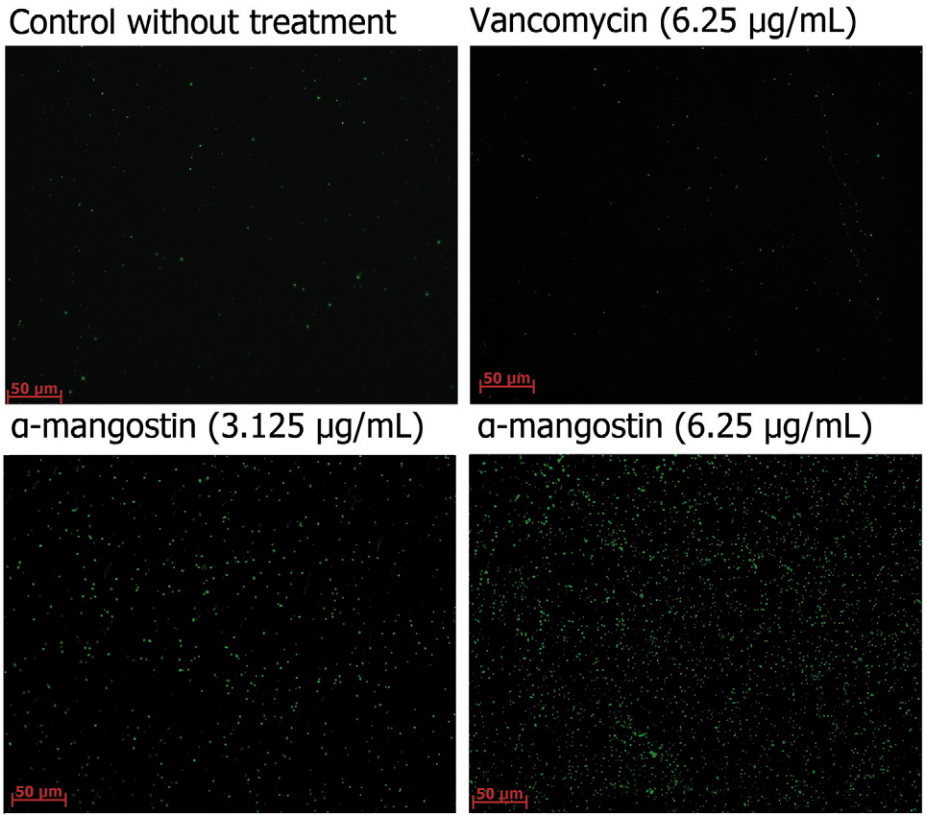

Fig. 8. α-Mangostin induced influx of SYTOX green into *S. aureus*. Cells fluoresced in green when treated with α-mangostin at 2× (3.125 μg/mL) and 4× MICs (6.25 μg/mL) as the consequent of membrane disruption. Control and vancomycin (6.25 μg/mL) did not show significant amount of stained cells. Control without treatment, cells with SYTOX green only.

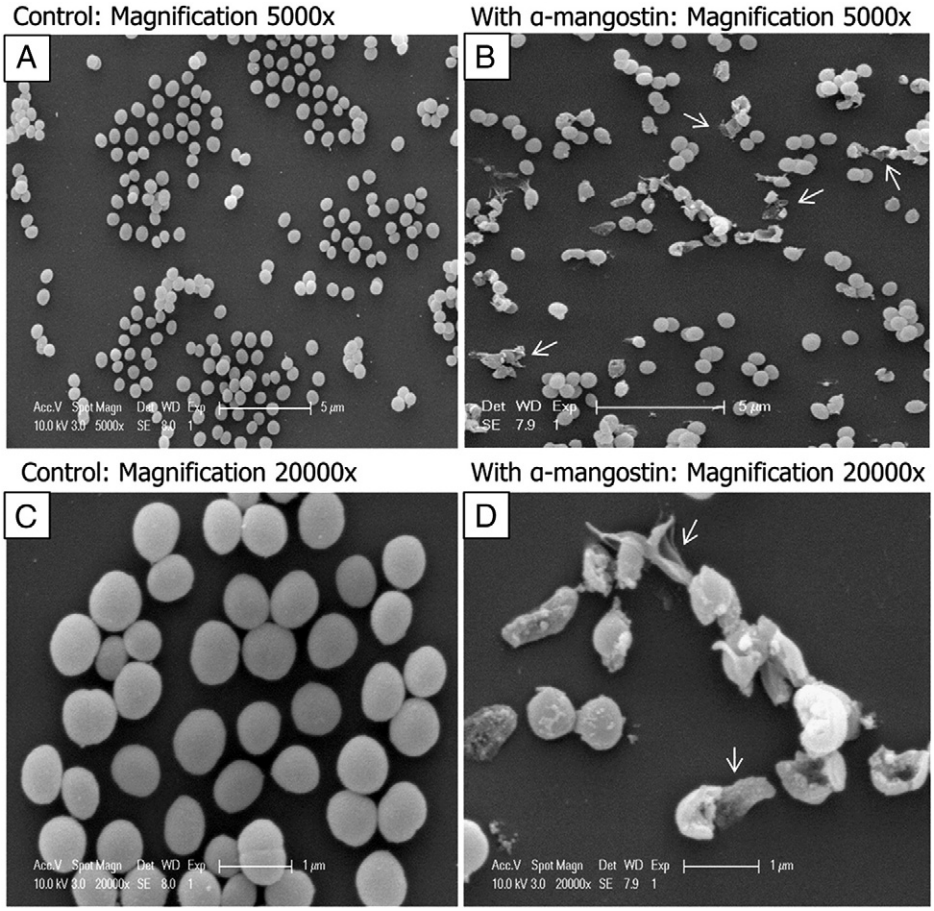

Fig. 9. Scanning electron microscopy showed that α-mangostin induced cell lysis and membrane disruption. Scanning electron microscopy of cell morphology of *S. aureus* with and without α-mangostin treatment after 30 min. (A) and (C): control without treatment at magnifications of 5000× and 20,000×, respectively. (B) and (D): *S. aureus* incubated with 10 μg/mL α-mangostin after 30 min at magnifications of 5000× and 20,000×, respectively. White arrow indicated leakage of intracellular components.

lipid bilayers (Fig. 11) decreased sharply by 100 ns and reached an equilibrium distance of 1.5 nm, locating just below the head groups of the lipid molecules. As the number of α-mangostin molecules was increased, some α-mangostin molecules penetrated deeper into the lower leaflet of the modeled bacterial membrane during the course of the simulation (Fig. 12). This was accompanied by perturbation of the integrity of the membrane with a large number of defects (filled with water molecules; Fig. 12) and the increased average lipid area (Fig. 13). These observations were strong indication of increased membrane perturbation induced by α-mangostin and which tended to corroborate the data from both the biophysical studies as well as the SEM results. Fig. 14 shows that the conformation of α-mangostin at different distances from the bilayer center. During penetration, the isoprenyl group first entered into the hydrophobic region of the membrane, which is driven by hydrophobic interactions. Then, the α-mangostin was entropically driven and its long axis was orientated in parallel to the lipid tails.

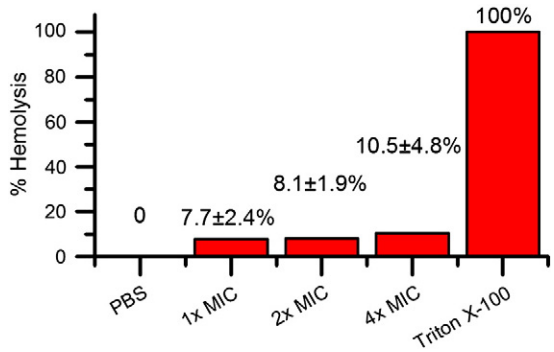

Fig. 10. Selectivity study using rabbit red blood cells. Hemolysis of α-mangostin at MIC and bactericidal concentrations were tested. PBS: indicator of no hemolysis; Triton X-100 (2%): indicator of 100% hemolysis.

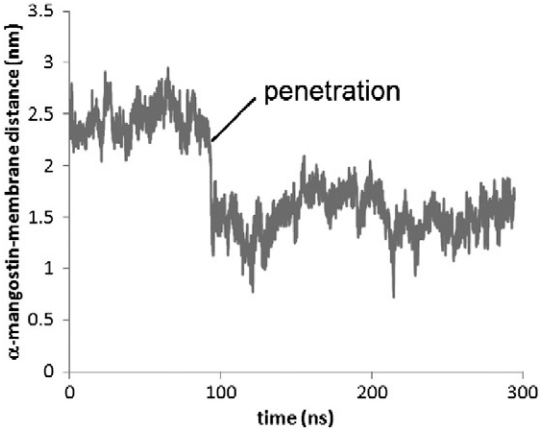

Fig. 11. α-Mangostin could penetrate into lipid bilayers rapidly. The distance between α-mangostin and the lipid bilayers decreased in 100 ns indicated α-mangostin could penetrate into the lipid bilayers rapidly.

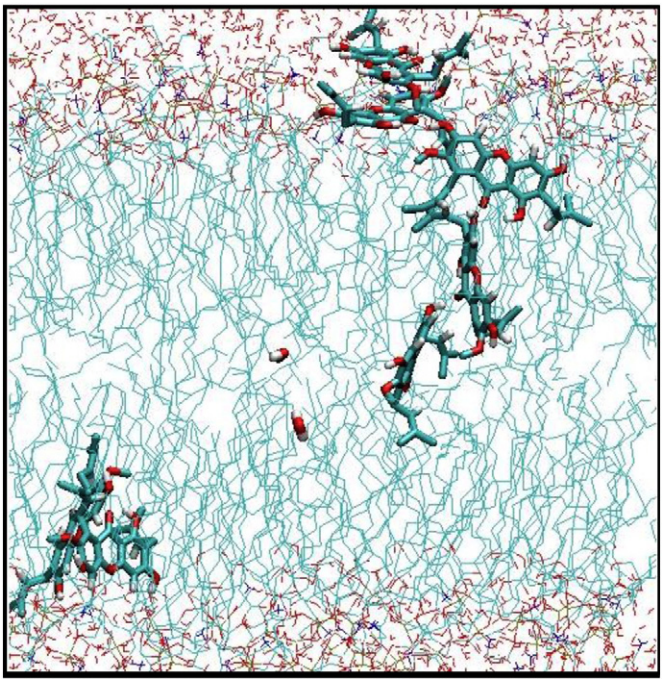

Fig. 12. Penetration of α-mangostin enhanced permeability of bacteria lipid membrane as a result of hydrophobic interaction. Snapshots of simulation at high α-mangostin concentration to show the interaction of α-mangostin with bacterial membrane (POPG/POPE = 75/25). At 200 ns, α-mangostin was able to reach lower leaflet of the lipid bilayers, which is facilitated by the hydrophobic interaction of the α-mangostin with phospholipid lipid tails. Penetration of α-mangostin also enhanced permeability of bacteria lipid membrane as water translocation across the membrane could be observed.

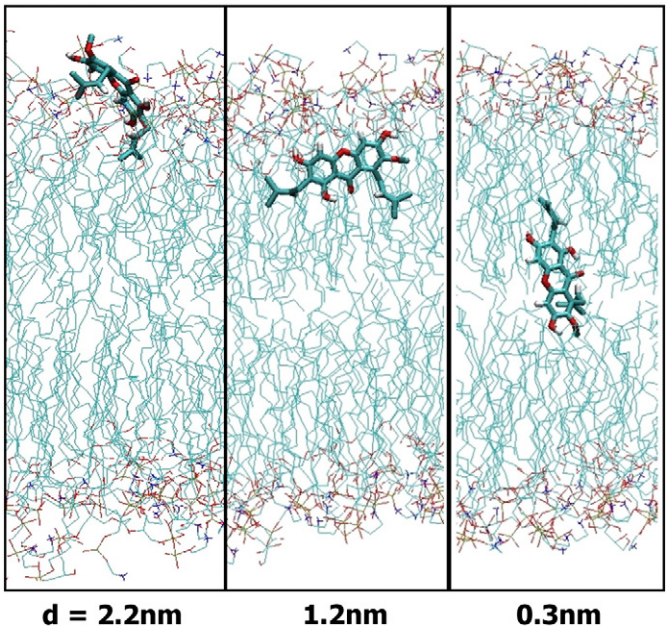

Fig. 14. The conformation of α-mangostin at different distance from the bilayer center. Isoprenyl group is important to facilitate the α-mangostin to penetrate into the lipid bilayer.

4. Discussion

In this study, the antimicrobial properties of five xanthones isolated from the hull of the mangosteen fruit (Fig. 1) were investigated. Among these compounds α-mangostin was found to be the most potent antimicrobial with rapid killing and low MIC values. The molecule elicits rapid *in vitro* bactericidal activity against Gram-positive bacteria including clinically relevant pathogens like MRSA (Table 1). The rapid bactericidal activity (3-log reduction in 5 min) of α-mangostin is reminiscent of membrane lytic cationic antimicrobial peptides [45,46]. In comparison, vancomycin did not display a 3-$\log_{10}$ reduction in viable bacteria count even after 300 min at a very high concentration of 8× MIC (Fig. 2C), a result in accordance with previous reports showing that 16–20 h was needed to achieve a 3-$\log_{10}$ reduction in viable bacteria counts [44]. It is generally accepted that vancomycin inhibits biosynthesis of the bacterial cell wall by binding to the D-Ala–D-Ala terminus of the growing peptidoglycan component, which is the substrate for crosslinking of peptidoglycan *via* the transpeptidation reaction, suggesting an inherently slower mechanism of action [47,48]. Thus, α-mangostin exhibits more potent and rapid bactericidal action as an outcome of membrane targeting compared to vancomycin.

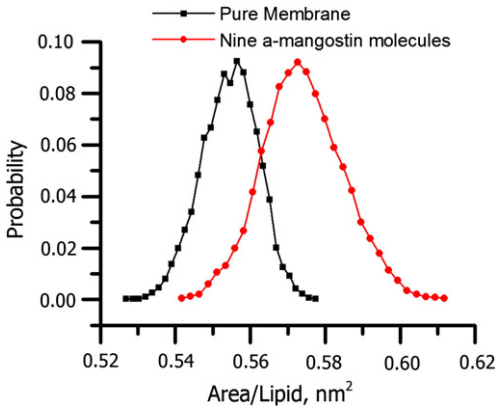

Fig. 13. Distribution of area per lipid of bacterial membrane in the presence of nine α-mangostin molecules using the last 200 ns MD simulation trajectories. The first 200 ns simulations were treated as equilibrium stage. The area per lipid was calculated by dividing the membrane area by the number of lipid molecules in one leaflet.

Interestingly, α-mangostin is a small organic molecule with a molecular weight of 410.46 g/mol which shares some similar antimicrobial properties with meta-phenylene ethynylene (mPE). mPE, a cationic antimicrobial peptide, mimics a membrane targeting small oligomer with rapid bactericidal activity. mPE also shows a low probability toward developing resistance in Gram-positive bacteria [49,50]. Our data indicates that α-mangostin targets the bacterial membrane, resulting in rapid bactericidal action and resistance is averted as the membrane targeting would be effective to reduce the mutational possibility of sufficiently changing the membrane structure to avoid resistance.

Although α-mangostin has been studied as an effective antimicrobial since the 1980s, the mechanism of action against Gram-positive bacteria remains unclear [11–16]. Using environment-sensitive fluorescent probes, we demonstrated that the primary target of the molecule is the cytoplasmic membrane. The $DiSC_3$-5 assay showed that α-mangostin induced a rapid dissipation of membrane potential at >2× MIC. To further investigate α-mangostin as a cytoplasmic membrane disruptive agent, we also showed that α-mangostin caused considerable leakage of intracellular components using EtBr uptake assay. In contrast, *S. aureus* exposed to daptomycin showed no increase in EtBr fluorescence. The result is in accordance with a report showing that daptomycin is a non-lytic membrane active agent [51]. The results were also supported by the SYTOX green assay and calcein leakage assays, which showed that α-mangostin could induce rapid bacterial membrane disruption. These results confirmed that α-mangostin alters the proton motive force and caused structural damage to the cytoplasmic membrane. Using SYTOX green with fluorescence microscopy further proved that α-mangostin could disrupt the cytoplasmic membrane. Significant cytoplasmic staining was observed at 4× MIC, which corresponded to the rapid 3-log reduction of viable cell count shown in Fig. 2A. Therefore, cytoplasmic membrane disruption is shown to be the dominant action

mechanism to explain the bactericidal properties of α-mangostin. Consistent with these results, SEM images showed that *S. aureus* exposed to α-mangostin had severely damaged morphology with irregular cell wall structure, leakage of intracellular components and agglomerated material, which corroborated the biophysical studies using $DiSC_3$-5, EtBr and SYTOX green. Interestingly, α-mangostin is also found as a membrane active agent to depolarize mitochondrion membrane potential in eukaryotic cells [52,53]. In fact, the mitochondrion membrane has similar lipid composition to the bacterial membrane with cardiolipin and phosphatidylethanolamine components [54]. Therefore, a similar mechanism of action maybe expected for michondrion and the bacterial membrane. Our data supports this statement as the antibacterial mechanism of α-mangostin disrupts the cell membrane.

The extent of membrane damage varied when bacteria were exposed to different membrane targeting antimicrobials. It has been suggested that the degree of membrane disruption is a continuous graduation [55]. The antimicrobial activity of α-mangostin appears to be different from other membrane targeted antimicrobials including cationic antimicrobial peptides [31], ceragenins [56] and daptomycin [57]. These agents elicit bactericidal action by forming ion channels or transmembrane pores without causing considerable damage to the membrane integrity [51,58]. However, it is important to note that membrane targeted action without causing lysis does not impede the emergence of drug resistant *S. aureus*. For instance, daptomycin resistant *S. aureus* has been reported recently [59–61]. Several groups reported genetic mutations in mprF, yycG, rpoB, and rpoC [62] and cell wall thickening [63] may play major roles in the emergence of daptomycin resistant *S. aureus*. In one particular mutant strain, it has been shown that resistance is mediated by over production of lysophosphotidyl glycerol. The lysophosphotidyl glycerol increases the net positive charge on the membrane surface thereby reducing the affinity of daptomycin and cationic antimicrobial peptides [64]. Therefore, interaction of α-mangostin with cytoplasmic membrane causing cell lysis *via* non-electrostatic interactions may represent a novel way of diminishing the probability of developing resistance in susceptible pathogens. In support of this, an *in vitro* multipassage resistance selection study has shown that no observable resistance was developed against α-mangostin. In contrast, Farrell et al. reported that resistance of bacteria emerged at the 5th passages against daptomycin.

Molecular dynamic simulations showed that a strong hydrophobic association of α-mangostin with lipid alkyl chains is the driving force for the rapid penetration of α-mangostin. The isoprenyl groups conjugated to the xanthone scaffold as short lipid tails were found to trigger the penetration into the hydrophobic region of the membrane. The isoprenyl groups would act to reduce the free energy barrier of penetration. In addition, the presence of isoprenyl groups further increased the hydrophobicity of α-mangostin, thus enhancing the tendency to partition into the membrane. All together, the presence of isoprenyl groups produced more potent antibacterial activity. The results suggest that the largely hydrophobic α-mangostin prefers to be solvated by the hydrophobic portion of the lipids. Lack of one isoprenyl group in SZ-1 and SZ-5 had poorer antimicrobial properties as the free energy barrier for bacterial membrane penetration was high. Our results are also in accordance with a recent report showing that the presence of at least two isoprenyl groups conjugated to the xanthone scaffold is important to confer potent antimicrobial properties [65]. In addition, during the simulations, we also observed a large number of water defects. Although some of these defects were transient, there were several occurrences of defects that evolved into water translocation across the membrane. At longer time and length scales, the increased permeability may allow large molecules to permeate through the membrane resulting in the leakage of intracellular components. It is likely that the strong affinity of α-mangostin to hydrophobic alkyl chain perturb the integrity and packing density, thus leading to the leakage of intracellular components. Although α-mangostin is also known to interact with transmembrane precursor proteins *via* hydrogen bonding [66], our biophysical studies and MD simulations demonstrate that the rapid perturbation of the bacterial inner membrane integrity is the main driver of cell killing. To further support the role of hydrophobic interaction of α-mangostin in perturbing bacterial membrane, we investigated the partition coefficient (logP) of α-mangostin using HPLC method according to the OECD guidelines for the testing of chemicals [67]. The determined logP value of α-mangostin was 6.4, indicating that α-mangostin has a strong hydrophobic nature and suggesting a strong tendency for partitioning into the bacterial membrane *via* hydrophobic interaction. Therefore, our data clearly suggests that hydrophobic interaction is crucial in bacterial killing.

In summary, we have shown that the bacteria inner membrane is the major target for α-mangostin in Gram-positive pathogens. α-Mangostin is easily extracted from the hull of a common tropical fruit. Elevated exposure of α-mangostin led to membrane disruption and leakage of intracellular contents within 5–10 min. Hydrophobic associations of α-mangostin with lipid membrane led to membrane deformation and diffusion of water molecules across the membrane. Resistance was not formed in laboratory simulations using *E. faecalis* and a MRSA. In addition, α-mangostin is more specific against bacterial membrane than mammalian membrane at MIC and bactericidal concentrations. Our results suggest that α-mangostin as a backbone molecule may be useful for further development.

Acknowledgements

This work was supported by NIG/NMRC/R753, NMRC/TCR/002-SERI/2088R618, BMRC-SCAMP-2/08/1/35/19/586R652 and Flagship funding X031. This work was also partially funded by Chinese National Science and Technology Major Project (No. 2009ZX09103-436) and Guangzhou Municipal Science and Technology Major Project (No. 2009A1-E011). We thank Li Mei Pang for her assistance and active discussion.

References

[1] R.H. Deurenberg, E.E. Stobberingh, The molecular evolution of hospital- and community-associated methicillin-resistant *Staphylococcus aureus*, Curr. Mol. Med. 9 (2009) 100–115.
[2] D.A. Talan, A. Krishnadasan, R.J. Gorwitz, G.E. Fosheim, B. Limbago, V. Albrecht, G.J. Moran, Comparison of *Staphylococcus aureus* from skin and soft-tissue infections in US emergency department patients, 2004 and 2008, Clin. Infect. Dis. 53 (2011) 144–149.
[3] G.J. Moran, A. Krishnadasan, R.J. Gorwitz, G.E. Fosheim, L.K. McDougal, R.B. Carey, D.A. Talan, Methicillin-resistant *S. aureus* infections among patients in the emergency department, N. Engl. J. Med. 355 (2006) 666–674.
[4] M.Z. David, R.S. Daum, Community-associated methicillin-resistant *Staphylococcus aureus*: epidemiology and clinical consequences of an emerging epidemic, Clin. Microbiol. Rev. 23 (2010) 616–687.
[5] J.A. Otter, G.L. French, Community-associated meticillin-resistant *Staphylococcus aureus* strains as a cause of healthcare-associated infection, J. Hosp. Infect. 79 (2011) 189–193.
[6] R.L. Skov, K.S. Jensen, Community-associated meticillin-resistant *Staphylococcus aureus* as a cause of hospital-acquired infections, J. Hosp. Infect. 73 (2009) 364–370.
[7] S.E. Cosgrove, Y. Qi, K.S. Kaye, S. Harbarth, A.W. Karchmer, Y. Carmeli, The impact of methicillin resistance in *Staphylococcus aureus* bacteremia on patient outcomes: mortality, length of stay, and hospital charges, Infect. Control Hosp. Epidemiol. 26 (2005) 166–174.
[8] F. von Nussbaum, M. Brands, B. Hinzen, S. Weigand, D. Habich, Antibacterial natural products in medicinal chemistry—exodus or revival? Angew. Chem. Int. Ed. Engl. 45 (2006) 5072–5129.
[9] J. Pedraza-Chaverri, N. Cárdenas-Rodríguez, M. Orozco-Ibarra, J.M. Pérez-Rojas, Medicinal properties of mangosteen (*Garcinia mangostana*), Food Chem. Toxicol. 46 (2008) 3227–3239.
[10] D. Obolskiy, I. Pischel, N. Siriwatanametanon, M. Heinrich, *Garcinia mangostana* L.: a phytochemical and pharmacological review, Phytother. Res. 23 (2009) 1047–1065.
[11] Y. Sakagami, M. Iinuma, K.G.N.P. Piyasena, H.R.W. Dharmaratne, Antibacterial activity of α-mangostin against vancomycin resistant enterococci (VRE) and synergism with antibiotics, Phytomedicine 12 (2005) 203–208.
[12] N. Boonnak, C. Karalai, S. Chantrapromma, C. Ponglimanont, H.-K. Fun, A. Kanjana-Opas, S. Laphookhieo, Bioactive prenylated xanthones and anthraquinones from *Cratoxylum formosum* ssp. pruniflorum, Tetrahedron 62 (2006) 8850–8859.
[13] S. Deachathai, W. Mahabusarakam, S. Phongpaichit, W.C. Taylor, Phenolic compounds from the fruit of *Garcinia dulcis*, Phytochemistry 66 (2005) 2368–2375.
[14] M. Iinuma, H. Tosa, T. Tanaka, F. Asai, Y. Kobayashi, R. Shimano, K. Miyauchi, Antibacterial activity of xanthones from guttiferaeous plants against methicillin-resistant *Staphylococcus aureus*, J. Pharm. Pharmacol. 48 (1996) 861–865.

[15] B.M. Sundaram, C. Gopalakrishnan, S. Subramanian, D. Shankaranarayanan, L. Kameswaran, Antimicrobial activities of *Garcinia mangostana*, Planta Med. 48 (1983) 59–60.
[16] W. Mahabusarakam, P. Wiriyachitra, S. Phongpaichit, Antimicrobial activities of chemical constituents from *Garcinia mangostana*, J. Sci. Soc. Thai. 12 (1986) 239–242.
[17] R. Kaomongkolgit, K. Jamdee, N. Chaisomboon, Antifungal activity of alpha-mangostin against *Candida albicans*, J. Oral Sci. 51 (2009) 401–406.
[18] P.T.M. Nguyen, R.E. Marquis, Antimicrobial actions of α-mangostin against oral streptococci, Can. J. Microbiol. 57 (2011) 217–225.
[19] P. Grohs, M.D. Kitzis, L. Gutmann, In vitro bactericidal activities of linezolid in combination with vancomycin, gentamicin, ciprofloxacin, fusidic acid, and rifampin against *Staphylococcus aureus*, Antimicrob. Agents Chemother. 47 (2003) 418–420.
[20] Y. Bai, S. Liu, P. Jiang, L. Zhou, J. Li, C. Tang, C. Verma, Y. Mu, R.W. Beuerman, K. Pervushin, Structure-dependent charge density as a determinant of antimicrobial activity of peptide analogues of defensin, Biochemistry 48 (2009) 7229–7239.
[21] S.P. Liu, L. Zhou, R. Lakshminarayanan, R.W. Beuerman, Multivalent antimicrobial peptides as therapeutics: design principles and structural diversities, Int. J. Pept. Res. Ther. 16 (2010) 199–213.
[22] J. Isaksson, B.O. Brandsdal, M. Engqvist, G.E. Flaten, J.S. Svendsen, W. Stensen, A synthetic antimicrobial peptidomimetic (LTX 109): stereochemical impact on membrane disruption, J. Med. Chem. 54 (2011) 5786–5795.
[23] Y. Zhang, Z. Song, J. Hao, S. Qiu, Z. Xu, Two new prenylated xanthones and a new prenylated tetrahydroxanthone from the pericarp of *Garcinia mangostana*, Fitoterapia 81 (2010) 595–599.
[24] X.J. Zhou, R.M. Huang, J. Hao, H.J. Huang, M.Q. Fu, Z.F. Xu, Y.M. Zhou, X.E. Li, S.X. Qiu, Two new prenylated xanthones from the pericarp of *Garcinia mangostana* (mangosteen), Helv. Chim. Acta 94 (2011) 2092–2098.
[25] G.J. Bennett, H.H. Lee, L.P. Lee, Synthesis of minor xanthones from *Garcinia mangostana*, J. Nat. Prod. 53 (1990) 1463–1470.
[26] S.X. Chen, M. Wan, B.N. Loh, Active constituents against HIV-1 protease from Garcinia mangostana, Planta Med. 62 (1996) 381–382.
[27] S. Sakai, M. Katsura, H. Takayama, N. Aimi, N. Chokethaworn, M. Suttajit, The structure of garcinone E, Chem. Pharm. Bull. (Tokyo) 41 (1993) 958–960.
[28] W. Mahabusarakam, P. Wiriyachitra, Chemical constituents of *Garcinia mangostana*, J. Nat. Prod. 50 (1987) 474–478.
[29] S. Suksamrarn, O. Komutiban, P. Ratananukul, N. Chimnoi, N. Lartpornmatulee, A. Suksamrarn, Cytotoxic prenylated xanthones from the young fruit of *Garcinia mangostana*, Chem. Pharm. Bull. (Tokyo) 54 (2006) 301–305.
[30] D.J. Farrell, M. Robbins, W. Rhys-Williams, W.G. Love, Investigation of the potential for mutational resistance to XF-73, retapamulin, mupirocin, fusidic acid, daptomycin, and vancomycin in methicillin-resistant *Staphylococcus aureus* isolates during a 55-passage study, Antimicrob. Agents Chemother. 55 (2011) 1177–1181.
[31] M. Wu, R.E. Hancock, Interaction of the cyclic antimicrobial cationic peptide bactenecin with the outer and cytoplasmic membrane, J. Biol. Chem. 274 (1999) 29–35.
[32] D. Liu, W.F. DeGrado, De novo design, synthesis, and characterization of antimicrobial beta-peptides, J. Am. Chem. Soc. 123 (2001) 7553–7559.
[33] Y. Jin, H. Mozsolits, J. Hammer, E. Zmuda, F. Zhu, Y. Zhang, M.I. Aguilar, J. Blazyk, Influence of tryptophan on lipid binding of linear amphipathic cationic antimicrobial peptides, Biochemistry 42 (2003) 9395–9405.
[34] Avanti Polar Lipids, Inc, Extrusion technique, http://www.avantilipids.com/index.php?option=com_content&view=article&id=1686&Itemid=405 assessed on 23 May 2012.
[35] Avanti Polar Lipids, Inc, determination of total phosphorus, http://www.avantilipids.com/index.php?option=com_content&view=article&id=1686&Itemid=405 accessed on 23 May 2012.
[36] D.E. Vance, J. Vance, Biochemistry of Lipids, Lipoproteins and Membranes, 2nd ed. Elsevier Science, Amsterdam, 1991.
[37] W. Zhao, T. Rog, A.A. Gurtovenko, I. Vattulainen, M. Karttunen, Role of phosphatidylglycerols in the stability of bacterial membranes, Biochimie 90 (2008) 930–938.
[38] C. Oostenbrink, A. Villa, A.E. Mark, W.F. van Gunsteren, A biomolecular force field based on the free enthalpy of hydration and solvation: the GROMOS force-field parameter sets 53A5 and 53A6, J. Comput. Chem. 25 (2004) 1656–1676.
[39] H. Berendsen, J. Postma, W.v. Gunsteren, J. Hermans, in: B. Pullman (Ed.), Intermolecular Forces, Reidel, Dordrecht, 1981.
[40] A.K. Malde, L. Zuo, M. Breeze, M. Stroet, D. Poger, P.C. Nair, C. Oostenbrink, A.E. Mark, An automated force field topology builder (ATB) and repository: version 1.0, J. Chem. Theory Comput. (2011) 111115094412000.
[41] P. Bjelkmar, P. Larsson, M.A. Cuendet, B. Hess, E. Lindahl, Implementation of the CHARMM force field in GROMACS: analysis of protein stability effects from correction maps, virtual interaction sites, and water models, J. Chem. Theory Comput. 6 (2010) 459–466.
[42] CLSI, Performance standards for antimicrobial susceptibility testing; twenty-first informational supplement, CLSI document M100-S21, 31, 2011.
[43] R.W. Finberg, R.C. Moellering, F.P. Tally, W.A. Craig, G.A. Pankey, E.P. Dellinger, M.A. West, M. Joshi, P.K. Linden, K.V. Rolston, J.C. Rotschafer, M.J. Rybak, The importance of bactericidal drugs: future directions in infectious disease, Clin. Infect. Dis. 39 (2004) 1314–1320.
[44] E.A. Coyle, M.J. Rybak, Activity of oritavancin (LY333328), an investigational glycopeptide, compared to that of vancomycin against multidrug-resistant Streptococcus pneumoniae in an in vitro pharmacodynamic model, Antimicrob. Agents Chemother. 45 (2001) 706–709.
[45] L.T. Nguyen, E.F. Haney, H.J. Vogel, The expanding scope of antimicrobial peptide structures and their modes of action, Trends Biotechnol. 29 (2011) 464–472.
[46] C.R. Dawson, A.F. Drake, J. Helliwell, R.C. Hider, The interaction of bee melittin with lipid bilayer membranes, Biochim. Biophys. Acta 510 (1978) 75–86.
[47] D.A. Beauregard, D.H. Williams, M.N. Gwynn, D.J. Knowles, Dimerization and membrane anchors in extracellular targeting of vancomycin group antibiotics, Antimicrob. Agents Chemother. 39 (1995) 781–785.
[48] C.W. Stratton, C. Liu, H.B. Ratner, L.S. Weeks, Bactericidal activity of deptomycin (LY146032) compared with those of ciprofloxacin, vancomycin, and ampicillin against enterococci as determined by kill-kinetic studies, Antimicrob. Agents Chemother. 31 (1987) 1014–1016.
[49] G.N. Tew, D. Clements, H. Tang, L. Arnt, R.W. Scott, Antimicrobial activity of an abiotic host defense peptide mimic, Biochim. Biophys. Acta 1758 (2006) 1387–1392.
[50] K. Nusslein, L. Arnt, J. Rennie, C. Owens, G.N. Tew, Broad-spectrum antibacterial activity by a novel abiogenic peptide mimic, Microbiology 152 (2006) 1913–1918.
[51] N. Cotroneo, R. Harris, N. Perlmutter, T. Beveridge, J.A. Silverman, Daptomycin exerts bactericidal activity without lysis of *Staphylococcus aureus*, Antimicrob. Agents Chemother. 52 (2008) 2223–2225.
[52] E. Martinez-Abundis, N. Garcia, F. Correa, S. Hernandez-Resendiz, J. Pedraza-Chaverri, C. Zazueta, Effects of alpha-mangostin on mitochondrial energetic metabolism, Mitochondrion 10 (2010) 151–157.
[53] A. Sato, H. Fujiwara, H. Oku, K. Ishiguro, Y. Ohizumi, Alpha-mangostin induces Ca^{2+}-ATPase-dependent apoptosis via mitochondrial pathway in PC12 cells, J. Pharmacol. Sci. 95 (2004) 33–40.
[54] R. Hovius, H. Lambrechts, K. Nicolay, B. de Kruijff, Improved methods to isolate and subfractionate rat liver mitochondria. Lipid composition of the inner and outer membrane, Biochim. Biophys. Acta 1021 (1990) 217–226.
[55] M. Dathe, T. Wieprecht, Structural features of helical antimicrobial peptides: their potential to modulate activity on model membranes and biological cells, Biochim. Biophys. Acta 1462 (1999) 71–87.
[56] R.F. Epand, J.E. Pollard, J.O. Wright, P.B. Savage, R.M. Epand, Depolarization, bacterial membrane composition, and the antimicrobial action of ceragenins, Antimicrob. Agents Chemother. 54 (2010) 3708–3713.
[57] J.A. Silverman, N.G. Perlmutter, H.M. Shapiro, Correlation of daptomycin bactericidal activity and membrane depolarization in *Staphylococcus aureus*, Antimicrob. Agents Chemother. 47 (2003) 2538–2544.
[58] X.Z. Lai, Y. Feng, J. Pollard, J.N. Chin, M.J. Rybak, R. Bucki, R.F. Epand, R.M. Epand, P.B. Savage, Ceragenins: cholic acid-based mimics of antimicrobial peptides, Acc. Chem. Res. 41 (2008) 1233–1240.
[59] M.K. Hayden, K. Rezai, R.A. Hayes, K. Lolans, J.P. Quinn, R.A. Weinstein, Development of daptomycin resistance in vivo in methicillin-resistant *Staphylococcus aureus*, J. Clin. Microbiol. 43 (2005) 5285–5287.
[60] L.Y. Hsu, M. Leong, M. Balm, D.S. Chan, P. Huggan, T.Y. Tan, T.H. Koh, P.Y. Hon, M.M. Ng, Six cases of daptomycin-non-susceptible *Staphylococcus aureus* bacteraemia in Singapore, J. Med. Microbiol. 59 (2010) 1509–1513.
[61] D.J. Skiest, Treatment failure resulting from resistance of *Staphylococcus aureus* to daptomycin, J. Clin. Microbiol. 44 (2006) 655–656.
[62] L. Friedman, J.D. Alder, J.A. Silverman, Genetic changes that correlate with reduced susceptibility to daptomycin in *Staphylococcus aureus*, Antimicrob. Agents Chemother. 50 (2006) 2137–2145.
[63] U. Bertsche, C. Weidenmaier, D. Kuehner, S.J. Yang, S. Baur, S. Wanner, P. Francois, J. Schrenzel, M.R. Yeaman, A.S. Bayer, Correlation of daptomycin resistance in a clinical *Staphylococcus aureus* strain with increased cell wall teichoic acid production and D-alanylation, Antimicrob. Agents Chemother. 55 (2011) 3922–3928.
[64] A. Peschel, R.W. Jack, M. Otto, L.V. Collins, P. Staubitz, G. Nicholson, H. Kalbacher, W.F. Nieuwenhuizen, G. Jung, A. Tarkowski, K.P. van Kessel, J.A. van Strijp, *Staphylococcus aureus* resistance to human defensins and evasion of neutrophil killing via the novel virulence factor MprF is based on modification of membrane lipids with l-lysine, J. Exp. Med. 193 (2001) 1067–1076.
[65] H.R.W. Dharmaratne, Y. Sakagami, K.G.P. Piyasena, V. Thevanesam, Antibacterial activity of xanthones from *Garcinia mangostana* (L.) and their structure–activity relationship studies, Nat. Prod. Res. (2012) 1–4.
[66] Y. Wang, Z. Xia, J.R. Xu, Y.X. Wang, L.N. Hou, Y. Qiu, H.Z. Chen, Alpha-mangostin, a polyphenolic xanthone derivative from mangosteen, attenuates beta-amyloid oligomers-induced neurotoxicity by inhibiting amyloid aggregation, Neuropharmacology 62 (2012) 871–881.
[67] OECD, Test No. 117: Partition Coefficient (n-Octanol/Water), HPLC Method, OECD Publishing, 2004.